Inorganic Chemistry

pubs.acs.org/IC

Article

$CuCu_3Fe_2Os_2O_{12}$: A Room-Temperature Ferrimagnet with Reduced Thermal Conductivity

Xiao Wang,* Fedor Temnikov, Xubin Ye, Maocai Pi, Zhao Pan, Weihao Li, Zhiwei Hu, Chien-Te Chen, Chang-Yang Kuo, Cheng Dong, Yao Shen, Wenmin Li, Sergey V. Streltsov,* and Youwen Long*

Cite This: *Inorg. Chem.* 2025, 64, 20796−20803

Read Online

ACCESS | Metrics & More | Article Recommendations

ABSTRACT: The transition-metal-only A- and B-site-ordered perovskite oxide $CuCu_3Fe_2Os_2O_{12}$ was successfully synthesized under high-pressure (18 GPa) and high-temperature (1475 K) conditions. The compound adopts a cubic lattice with the charge configuration $Cu^{+}Cu_3^{2+}Fe_2^{3+}Os_2^{5.5+}O_{12}$, in which $Cu(1)^{+}$ and $Cu(2)^{2+}$ exhibit a 1:3 ordering at the A-site and Fe^{3+} and $Os^{5.5+}$ arrange in a rock-salt-type ordered pattern at the B-site. A ferrimagnetic transition is found to occur at 290 K due to magnetic interactions among the corner-shared $Cu(2)O_4$ planar squares, FeO_6 octahedra, and OsO_6 octahedra. Low-temperature specific heat data suggest the presence of itinerant electronic behavior, in agreement with the half-metallic electronic band structure calculated in theory. Different from most itinerant electronic systems, the current $CuCu_3Fe_2Os_2O_{12}$ shows unusually low thermal conductivity (1.4 W K^{-1} m^{-1} at 300 K) since the small-size A-site $Cu(1)^{+}$ ions "rattle" within large cuboctahedron units along the [111] direction. This study opens up a new way to design metallic conductive materials with unusually low thermal conductivity in perovskite oxides.

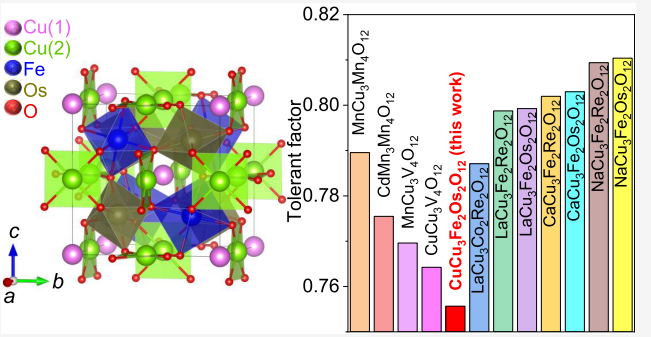

1. INTRODUCTION

The A- and B-site-ordered quadruple perovskite oxide $AA'_3B_2B'_2O_{12}$ offers a versatile platform for exploring multifunctional materials due to its ability to accommodate magnetic transition-metal ions at distinct sublattices. As illustrated in Figure 1a, this ordered structure originates from the ABO_3 perovskite framework, where three-quarters of the A sites are substituted with Jahn−Teller cations (A′), forming $A'O_4$ planar squares, while the B and B′ ions arrange in a rock-salt-type ordered pattern. The network of corner-shared $A'O_4$ squares, BO_6 octahedra, and $B'O_6$ octahedra form a robust lattice. Interactions between adjacent cations lead to emergent phenomena such as charge ordering,[1] multiferroicity,[2] colossal magnetoresistivity,[3] half-metallicity,[4] metal−insulator transition,[5] and electrocatalysis.[6]

The $ACu_3Fe_2Os_2O_{12}$ family (A = Na, Ca, and La) has been extensively investigated.[7−10] Strong magnetic couplings between Cu, Fe, and Os result in a ferrimagnetic (FiM) spin alignment of Cu(↑)Fe(↑)Os(↓) characterized by high Curie temperatures. Furthermore, the nonmagnetic A-site influences the valence state of Os, thereby modifying the electronic band structure. For $Os^{4.5+}$ (A = La^{3+}) and Os^{5+} (A = Ca^{2+}), the Fermi level is located at the top of the valence band, resulting in semiconducting or insulating ground states. In contrast, the $Os^{5.5+}$ (A = Na^{+}) counterpart lowers the Fermi level within the spin-down valence band, forming a half-metallic state.

While the A-site typically hosts large ions such as alkaline, alkaline earth, or rare-earth elements, introducing small transition-metal ions into the A-site is an intriguing possibility due to the potential for novel electronic and magnetic interplay among multiple *d* orbitals. However, as illustrated in Figure 1b, the small ionic radius of a transition metal A ion leads to tolerance factors[11] ($t = r_{A-O}/\sqrt{2}\, r_{B-O}$) far below the ideal value of 1, significantly increasing the structural instability.[12−15] To date, only a limited number of transition-metal-only simple perovskites,[16,17] double perovskites,[18−23] and A-site ordered perovskites[24−26] have been successfully synthesized.

In this study, we report synthesizing the transition-metal-only A- and B-site-ordered perovskite oxide $CuCu_3Fe_2Os_2O_{12}$ (CCFOO) under high-pressure conditions of 18 GPa. The B′-site of $Os^{5.5+}$ is strongly antiferromagnetically (AFM) coupled

Received: August 8, 2025
Revised: September 23, 2025
Accepted: September 26, 2025
Published: October 7, 2025

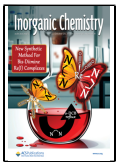

Downloaded via INST OF PHYSICS on November 10, 2025 at 05:23:44 (UTC).
See https://pubs.acs.org/sharingguidelines for options on how to legitimately share published articles.

ACS Publications

© 2025 American Chemical Society

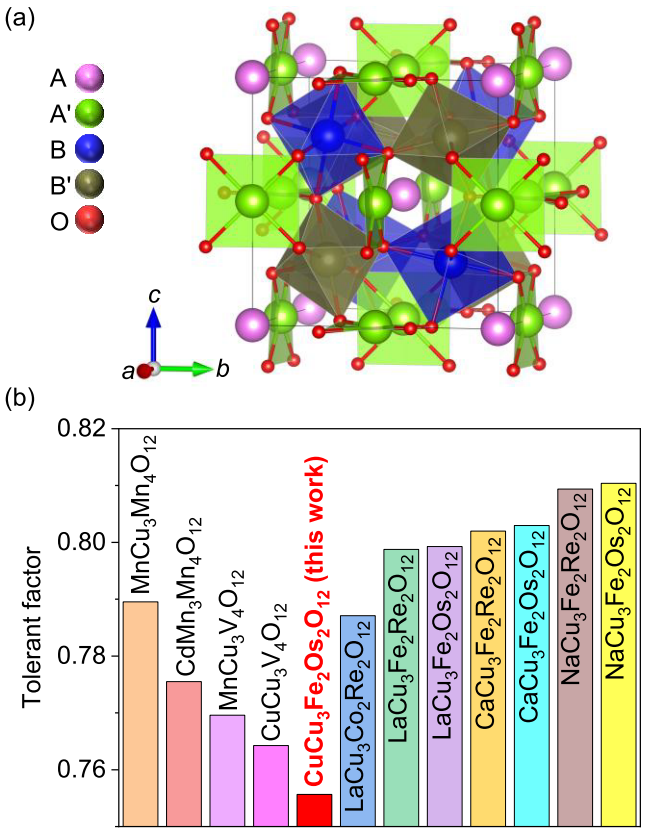

Figure 1. (a) Crystal structure of A- and B-site-ordered perovskite oxide $AA'_3B_2B'_2O_{12}$. The A, A′, B, B′, and O atoms are shown in magenta, green, blue, brown, and red, respectively. (b) Tolerant factor of CCFOO and some quadruple perovskite oxide analogues.

with the B-site Fe^{3+} and A′-site $Cu(2)^{2+}$, leading to a FiM transition at 290 K. The Fermi surface resides within the minority valence band, while a wide band gap of 1.4 eV opens in the majority band, indicating a half-metallic ground state. The nonmagnetic A-site $Cu(1)^{+}$ ($3d^{10}$) was also identified. Remarkably, on account of that the A-site is occupied by a small Cu atom, a t value of 0.75 is realized, which is the smallest among the quadruple perovskite oxides to the best of our knowledge (Figure 1b). This significant lattice mismatch gives rise to an unusual elongation of the Cu(1)−O bond. This under-bonded Cu(1) forms a "rattling" or phonon-glass state,[25,27,28] leading to an unusually low thermal conductivity of 1.4 W K^{-1} m^{-1} at room temperature.

2. EXPERIMENTAL AND THEORETICAL CALCULATIONS

High purity (>99.9%) CuO, Fe_2O_3, and Os powder in a mole ratio of 4:1:2, with an appropriate amount of $KClO_4$ as an oxidizing agent, were thoroughly ground in an agate mortar and the mixture powder was sealed into a platinum capsule. These procedures were carried out in a glovebox full of argon gas. Then, the capsule was processed with a Max Voggenreiter Walker-type multianvil apparatus. The pressure was slowly increased to 18 GPa in 5 h, after which the temperature was increased to 1475 K in 10 min and maintained for 30 min. Then, the temperature was quenched to room temperature in a few seconds and the pressure was slowly released to ambient pressure in 24 h. The residual KCl was then rinsed with deionized water.

Powder synchrotron X-ray diffraction (SXRD) was collected at the BL02B2 (λ = 0.80 Å) beamline of SPring-8. The 2θ scan was adopted from 5 to 75° with a step of 0.006°. The Rietveld refinement[29] was performed using the GSAS software.[30] The X-ray absorption spectra (XAS) at the Cu-$L_{2,3}$ and Fe-$L_{2,3}$ edges were obtained at room temperature at the TLS11A beamline of the National Synchrotron Radiation Research Center (NSRRC) using the total electron yield mode. The XAS at the Os-L_3 edge was obtained at the TLS17C beamline of the NSRRC by using a transmission mode. The magnetic measurements were performed using a Quantum Design superconducting quantum interference device magnetometer (MPMS-VSM). Both zero-field-cooling (ZFC) and field-cooling (FC) modes were adopted under a magnetic field of 0.1 T. The electrical resistivity was measured using a Quantum Design physical property measurement system (PPMS) with a standard four-probe method. The thermal conductivity and specific heat were measured using PPMS.

The calculations of density functional theory were performed with the projector augmented plane-wave basis, which is implemented in the Vienna *ab initio* simulation package.[31] And the plane-waves are cutoff at 550 eV. The exchange−correlation of electrons is described by the generalized gradient approximation with the form proposed by Perdew, Burke, and Ernzerhof.[32] To improve the descriptions on the correlation interactions, the Hubbard U scheme[33,34] is employed with U_{eff} = 5, 4, and 2 eV applied on the d-shell of Cu, Fe, and Os (so-called DFT + U method). The energy converge criterion for solving self-consistent Kohn−Sham equations is 10^{-7} eV. The Brillouin zone is sampled with the Γ-center and resolution better than 0.03 $Å^{-1}$ mesh, using the scheme of Monkhorst−Pack.[35] All of the structures in this study are fully relaxed until the Hellmann−Feynman is smaller than 0.02 eV $Å^{-1}$.

3. RESULTS AND DISCUSSION

Figure 2 presents the SXRD pattern of CCFOO. The appearance of $h + k + l$ = odd Bragg peaks such as (111), (311), and (333) confirms the formation of rock-salt-type ordering between Fe and Os. The SXRD data are well-fitted using the $Pn-3$ (No. 201) space group with a = 7.4426(2) Å, with the corresponding crystal structure depicted in Figure 1a. Several remaining Fe_2O_3 and OsO_2 of 4 and 2 wt % were identified, respectively, and 14% Fe/Os antisite occupation was observed. The refined structural parameters are summarized in Table 1. Bond valence sum (BVS)[36] calculations based on the bond lengths yield the valence states: $Cu(1)^{0.6+}$, $Cu(2)^{2.1+}$, $Fe^{2.8+}$, and $Os^{5.4+}$. Notably, the under-bonded Cu(1), situated within a large cuboctahedron cage, adopts a nonmagnetic Cu^{+} ($3d^{10}$) state due to the anomalously elongated Cu−O bond of 2.72 Å. Additionally, the thermal factor of the Cu(1) is an

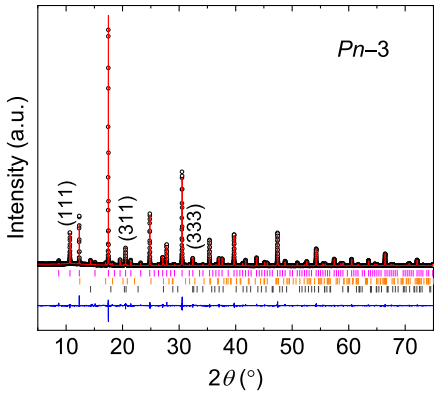

Figure 2. SXRD pattern and Rietveld refinement of CCFOO. The black circles, red lines, and blue lines indicate the observed, calculated, and difference, respectively. The magenta ticks indicate the allowed Bragg reflections for space group $Pn-3$. The orange and gray ticks, respectively, indicate the allowed Bragg reflection of the minor Fe_2O_3 ($R-3c$) and OsO_2 ($P4_2/mnm$) impurities.

https://doi.org/10.1021/acs.inorgchem.5c03691
Inorg. Chem. 2025, 64, 20796−20803

Table 1. Structural Parameters CCFOO, with Space group *Pn*−3 (No. 201) and the Wyckoff Positions Cu(1) 2*a* (0.25, 0.25, 0.25), Cu(2) 6*d* (0.25, 0.75, 0.75), Fe 4*b* (0, 0, 0), Os 4*c* (0.5, 0.5, 0.5), and O 24*h* (*x*, *y*, *z*)[a]

parameters	values
a (Å)	7.4426(2)
x (O)	0.2597(6)
y (O)	0.4380(9)
z (O)	0.5637(9)
G (4*b* for Fe)	0.860(1)
G (4*c* for Os)	0.860(1)
G (4*c* for Fe)	0.140(1)
G (4*b* for Os)	0.140(1)
U_{iso} [Cu(1)] (100 × Å^2)	9.82(26)
U_{iso} [Cu(2)] (100 × Å^2)	0.23(4)
U_{iso} (Fe) (100 × Å^2)	0.42(4)
U_{iso} (Os) (100 × Å^2)	0.36(3)
U_{iso} (O) (100 × Å^2)	1.27(12)
$d_{Cu(1)-O}$ (Å) (×12)	2.723(8)
$d_{Cu(2)-O}$ (Å)	1.971(4) (×4)
	2.706(8) (×4)
	3.294(4) (×4)
d_{Fe-O} (Å) (×6)	2.043(4)
d_{Os-O} (Å) (×6)	1.907(4)
∠Fe−O−Os (°)	140.8(2)
BVS [Cu(1)]	0.59
BVS [Cu(2)]	2.12
BVS (Fe)	2.83
BVS (Os)	5.40

[a]The BVS values (V_i) were calculated using the formula $V_i = \sum_j S_{ij}$, where $S_{ij} = \exp[(r_0 - r_{ij})/0.37]$. The values of r_0 are 1.610 for Cu^+, 1.679 for $Cu2^+$, 1.765 for Fe^{3+}, and 1.868 for Os^{5+}. The parameter G represents the site occupancy. R_{wp} = 7.71%, R_p = 5.66%.

order of magnitude larger than that of other sites, indicative of a "rattling" state,[25] which is discussed in detail later.

XAS measurements were conducted to verify the valence states in CCFOO experimentally. For transition metals, XAS at the $L_{2,3}$ edges is highly sensitive to the valence states and the local environments. Specifically, in an open *d*-shell system, an increase of one in valence state typically induces a 1−2 eV shift in the white line of the spectrum toward higher photon energy, alongside notable changes in peak features.[7,37]

The Cu-$L_{2,3}$ XAS results, along with reference compounds,[38,39] are illustrated in Figure 3a. The white line of CCFOO closely resembles that of CuO, and the L_3 peak aligns with the energy of CuO, indicating a 2+ valence state for Cu(2). Oscillations following the Cu-L_3 peak resemble contributions from the conduction band, observed in metallic oxides,[4,8] suggesting a metallic nature for CCFOO. However, due to the fully filled 3*d* orbital of Cu^+, the L_3 peak intensity for Cu^+ is approximately one-third of that of Cu^{2+}.[40] Given the 1:3 ratio of A and A′ sites, the L_3 XAS intensity of $Cu(1)^+$ in CCFOO is expected to be about one-ninth that of $Cu(2)^{2+}$. Consequently, the weak $Cu(1)^+$ signal is obscured by oscillation following the $Cu(2)^{2+}$-L_3 XAS peak. The Fe-$L_{2,3}$ XAS of CCFOO illustrated in Figure 3b closely matches that of Fe_2O_3, with the L_3 peak located at 1 eV higher in energy compared to FeO, confirming a 3+ valence state for Fe. Similarly, The Os-L_3 XAS spectrum, displayed in Figure 3c, is compared with references for Os^{4+} in (La_2MgOsO_6),[9] via 5+ in ($CaCu_3Fe_2Os_2O_{12}$),[7] to Os^{6+} (Ba_2NiOsO_6).[41] With the Os

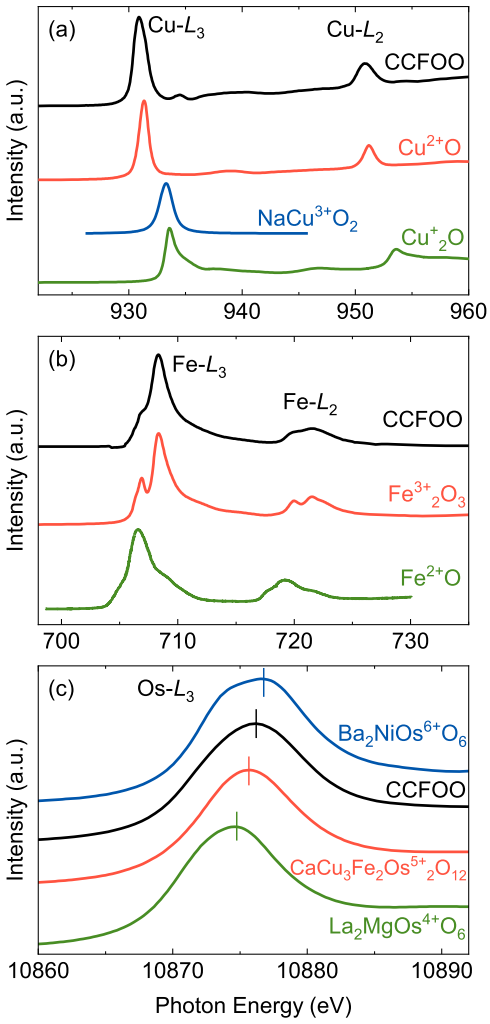

Figure 3. XAS at the (a) Cu-$L_{2,3}$, (b) Fe-$L_{2,3}$, and (c) Os-L_3 edges of CCFOO. The XAS of some references is displayed.

valence increasing from 4+ to 6+, the L_3 white line shifts progressively to higher energies. For CCFOO, the Os-L_3 peak lies between the Os^{5+} and the Os^{6+} references, indicating an average valence of $Os^{5.5}$. Thus, both BVS calculations and XAS measurements consistently determine the valence configuration of CCFOO as $Cu^+Cu_3{}^{2+}Fe_2{}^{3+}Os_2{}^{5.5+}O_{12}$, which is in agreement with the charge conservation principles.

Now, we turn to investigate the magnetic properties of CCFOO. As illustrated in Figure 4a, both the ZFC and FC curves of the temperature-dependent magnetic susceptibility (χ) exhibit a pronounced increase near $T_C \sim 290$ K, indicating a ferromagnetic (FM) or FiM transition. Upon further cooling, the ZFC and FC curves gradually diverge due to different moments in a FiM arrangement, magnetic domains, and/or magnetic frustration arising from Fe/Os antisite occupancy. Figure 4b displays the reciprocal magnetic susceptibility of the ZFC curve, which follows the Curie−Weiss law at 300−350 K, expressed as $(\chi - \chi_0)^{-1} = (T - \theta)/C$, with a Weiss temperature θ = 277 K. The positive θ indicates dominant FM interactions in CCFOO, and the value of θ closely matches the experimental T_C. The effective magnetic moment, derived from the Curie constant C = 10.79 emu mol^{-1}, is calculated to be $\mu_{eff} = \sqrt{8C} = 9.29\ \mu_B$ f.u.$^{-1}$. The value of μ_{eff} is in good agreement with the theoretical spin-only value of $\mu_{eff} = g\sqrt{\sum_i S_i(S_i + 1)} = 10.07\ \mu_B$ f.u.$^{-1}$, considering three $Cu(2)^{2+}$

https://doi.org/10.1021/acs.inorgchem.5c03691
Inorg. Chem. 2025, 64, 20796−20803

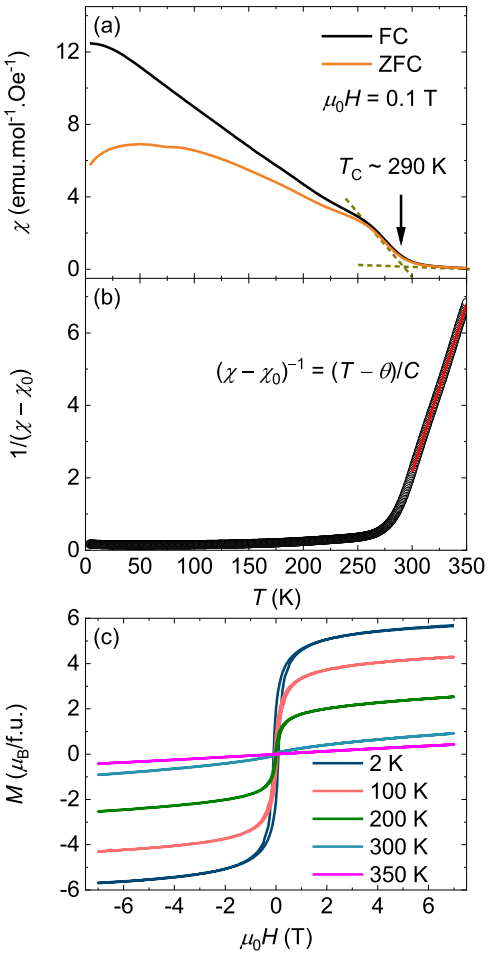

Figure 4. (a) Temperature-dependent magnetic susceptibility of CCFOO. (b) The inversed magnetic susceptibility (black circles) and the Curie–Weiss fitting at 300–350 K with the formula $(\chi - \chi_0)^{-1} = (T - \theta)/C$. (c) Field-dependent magnetization of CCFOO at selected temperatures.

($3d^9$, S = 1/2), two Fe^{3+} ($3d^5$, S = 5/2), and two $Os^{5.5+}$ ($5d^{3.5}$, S = 2.5/2), with the Landé g factor of 2. It is worth noting that the $Cu(1)^+$ with $3d^{10}$ configuration is nonmagnetic. The slight reduction in the experimental value can be attributed to spin–orbit coupling effects of Os.

Figure 4c illustrates the field-dependent magnetization measured at various temperatures. Above T_C, such as at 350 K, the magnetization varies linearly with the applied magnetic field, indicative of a paramagnetic state. Below T_C, coercive behavior emerges, with the saturated magnetization reaching 5.7 μ_B f.u.$^{-1}$ at 2 K and 7 T. Considering the spin-only scheme of $Cu(2)^{2+}$ (S = 1/2), Fe^{3+} (S = 5/2), and $Os^{5.5+}$ (S = 2.5/2), the spin configuration of Cu(2)(↑)Fe(↑)Os(↓) with a theoretic value of 8 μ_B f.u.$^{-1}$ aligns closely with experimental observations, consistent with the behavior of $ACu_3Fe_2Os_2O_{12}$ (A = Na, Ca and La) compounds, where AFM coupling between Cu(2)/Fe and Os dominates.[7−10] The small discrepancy likely arises from Fe/Os antisite disorder.

The temperature-dependent electrical resistivity of CCFOO is presented in Figure 5a. The resistivity, on the order of 1 Ω cm^{-1}, increases slightly upon cooling, suggesting the presence of grain boundary effects typical of polycrystalline metals.[4,8] Moreover, the electrical conductivity is influenced by an applied magnetic field. Figure 5a also illustrates the magneto-

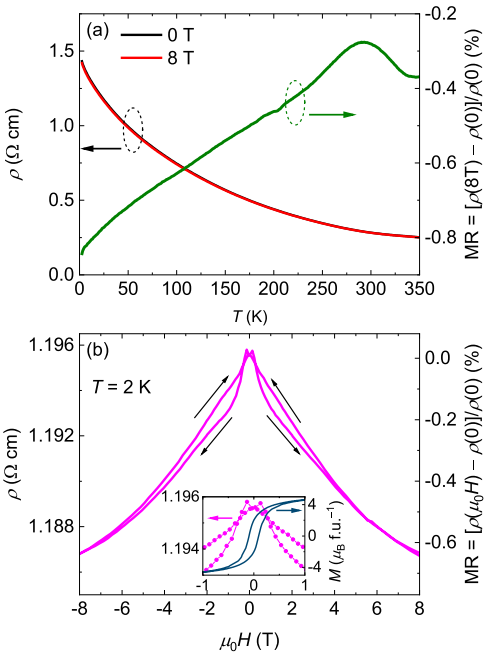

Figure 5. (a) Temperature-dependent resistivity and MR of CCFOO. (b) Field-dependent resistivity and MR of CCFOO at 2 K. The inset displays the resistivity and magnetization within a ± 1 T magnetic field.

resistance (MR) under an 8 T field, calculated as (MR = $[\rho(8T) - \rho(0)]/\rho(0) \times 100\%$) as a function of the temperature. A notable anomaly in the MR near T_C corresponds to the second-order FiM transition of CCFOO.

To further explore the MR effect, field-dependent MR was measured at 2 K. As illustrated in Figure 5b, the electrical resistivity decreases with increasing field as the applied magnetic field gradually aligns spins parallelly. However, the field-dependent MR also exhibits coercive behavior, with a maximum observed at nonzero magnetic fields, producing a butterfly-shaped MR curve. The MR behavior between ± 1 T is depicted in the inset of Figure 5b. At the coercive field of the $M(H)$ curve, the MR reaches its maximum. This behavior indicates a spin-valve-type electrical transport mechanism, which is commonly associated with the half-metallicity of metallic oxides.[4,12,42]

Distinct from the corner-shared $Cu(2)O_4$ square planar units and Fe/OsO_6 octahedra, which are strongly correlated magnetically and electrically, the A-site in typical perovskites is highly isolated within a hollow cuboctahedron accommodating large nonmagnetic ions.[1−10] However, in the present CCFOO, despite the small ionic radius of $Cu(1)^+$, an unusually elongated Cu(1)–O bond as long as 2.723(8) Å has been observed (Table 1). This under-bonded Cu(1) ion, coupled with its high thermal factor, is reminiscent of a phonon-glass or "rattling" state.[25,27,28] In such a state, thermal transport is significantly impeded and a low thermal conductivity is expected. Figure 6 illustrates the temperature-dependent thermal conductivity (λ) of CCFOO. Across the measured range of 2–380 K, CCFOO exhibits exceptionally low λ values, approximately 2 orders of magnitude smaller than those of metallic elements. At room temperature, the thermal conductivity is as low as 1.4 W K^{-1} m^{-1}, a value lower than other metallic oxides with reduced thermal conductivity, such as $NaCo_2O_4$ (2.1 W K^{-1} m^{-1}),[43] $Ba_2Sr_2Co_2O_y$ (2.1 W K^{-1}

https://doi.org/10.1021/acs.inorgchem.5c03691
Inorg. Chem. 2025, 64, 20796−20803

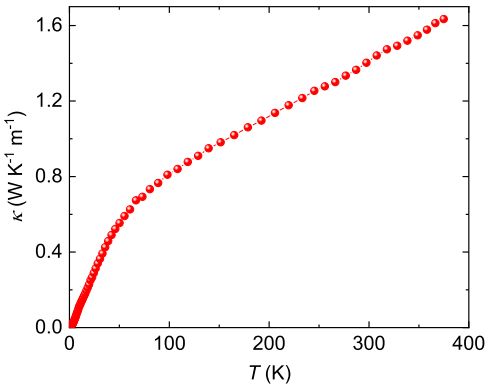

Figure 6. Temperature-dependent thermal conductivity of CCFOO.

m^{-1}),[44] $Cd_2Os_2O_7$ (1.8 W K^{-1} m^{-1}),[45] and $NaMn_{0.77}O_2$ (1.5 W K^{-1} m^{-1}).[46] While the low thermal conductivity in these materials is typically attributed to phonon scattering within low-dimensional structures, such as CoO_2 layers, the reduced λ in CCFOO arises from the significant rattling of the Cu(1) sublattice[25] despite the lattice maintaining cubic symmetry. This result suggests a unique approach for achieving isotropic low thermal conductivity within three-dimensional networks.

The specific heat (C_P) of CCFOO was further analyzed, as illustrated in Figure 7. At high temperatures, C_P approaches its

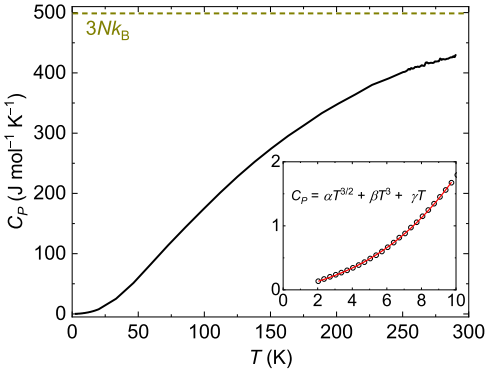

Figure 7. Temperature-dependent heat capacity of CCFOO. The inset displays the heat capacity below 10 K (black circles) and the fitting with the formula $C_P = \alpha T^{3/2} + \beta T^3 + \gamma T$ (red line).

theoretical Dulong–Petit limit $3Nk_B$ = 499 J mol^{-1} K^{-1}, where $N = 20N_A$ represents the number of atoms in the formula unit, $N_A = 6.022 \times 10^{23}$ mol^{-1} is Avogadro's constant, and $k_B = 1.381 \times 10^{-23}$ J K^{-1} is the Boltzmann constant. At low temperatures, as depicted in the inset of Figure 7, the specific heat data can be fitted using the equation $C_P = \alpha T^{3/2} + \beta T^3 + \gamma T$ for temperatures below 10 K. The fitting parameters are α = 14.6 mJ mol^{-1} $K^{-5/2}$, β = 0.90 mJ mol^{-1} K^{-4}, and γ = 4.18 mJ mol^{-1} K^{-2}, indicating that FM excitations, phonons, and electrons contribute to the heat capacity.

First-principles calculations were performed to gain deeper insight into CCFOO. We started by analyzing the electronic and magnetic properties. The optimized lattice parameter after full relaxation is 7.4598 Å, in accordance with the refined results shown in Table 1. The calculated band structure and density of states, depicted in Figure 8, confirm that for the Cu(1) site, the e_g bands of both spin channels are fully occupied and energetically degenerate, consistent with the nonmagnetic $Cu(1)^+$ state featuring a completely filled $3d^{10}$ orbital. Moreover, the Fermi level (E_F) intersects the valence band of the down-spin channel while residing within the band gap of the up-spin channel, confirming the half-metallic nature of CCFOO. The up-spin channel exhibits a wide band gap of 1.4 eV, indicating a stable half-metallic state resistant to thermally excited spin flipping.[47]

Next, we study possible rattling in CCFOO. Similar to $CuCu_3Fe_2Re_2O_{12}$,[48] we investigated various directions of rattling distortions. Displacements along crystal axes, such as [001], or within planes, such as [011], are found to be energetically less favorable than those along the [111] direction, as depicted in Figure 9a. It is important to note that not all [111]-type directions are equivalent. The unit cell contains two Cu(1) ions, allowing for several distinct displacement scenarios: both Cu(1) ions displaced toward Fe ions, both toward Os ions, and one toward Fe and the other toward Os. Among these, the configuration in which both Cu(1) ions are displaced toward Fe ions yields the lowest total energy, as depicted in Figure 9b. Interestingly, this agrees with the simplest ionic consideration based on the energy gain due to Coulomb repulsion: $Cu(1)^+$ ions can more easily approach Fe^{3+} rather than to $Os^{5.5+}$ (however, we stress that this material is a metal and other contributions have to be taken into account). The displacement magnitude of Cu(1) ions in CCFOO is approximately 0.5–0.6 Å, which is comparable to that calculated in $CuCu_3Fe_2Re_2O_{12}$,[48] where the Cu(1)–O bond length of 2.723 Å is slightly shorter than the latter (2.763 Å). Moreover, the energy minimum is about 10 meV lower.

The vibrational frequency of the Cu(1) ion in the harmonic approximation near the displacement potential minimum was estimated.[25,49,50] The potential shown in Figure 9 was fitted by using a quartic polynomial via the least-energy method and then expanded into a Taylor series around the minimum at approximately 0.55 Å. The coefficient in front of the quadratic term $(x-x_0)^2$, $(1/2)f''(x_0)$, defines the force constant k. The resulting vibrational frequency of this rattling mode is about 40 cm^{-1} (1.2 THz).

4. CONCLUSIONS

The novel transition-metal-only A- and B-site-ordered perovskite oxide $CuCu_3Fe_2Os_2O_{12}$ was synthesized under high-pressure and high-temperature conditions. This compound crystallizes in the cubic $Pn\bar{3}$ space group with $Cu(1)^+$ and $Cu(2)^{2+}$, respectively, occupying the A and A′ sites in a 1:3 order, and Fe^{3+} and $Os^{5.5+}$ occupying the B and B′ sites in a rock-salt order. The material exhibits room-temperature ferrimagnetism at a Curie temperature of 290 K. A spin-valve-type MR was observed at low temperatures, indicative of half-metallicity, which was further corroborated by first-principles calculations revealing a wide majority band gap of 1.4 eV. The ferrimagnetic and half-metallic properties are attributed to the interconnected network formed by the corner-shared $Cu(2)O_4$ square planar units and Fe/OsO_6 octahedra. Meanwhile, the isolated A-site $Cu(1)^+$ situated within an unusually expanded $Cu(1)O_{12}$ cuboctahedron undergoes a "rattling" state, leading to a low thermal conductivity of 1.4 W K^{-1} m^{-1} at room temperature. Thus, by tuning the properties of various sublattices, $CuCu_3Fe_2Os_2O_{12}$ integrates multiple physical properties, including room-temperature magnetization, half-metallicity, and low thermal conductivity, into a single phase. This work provides a novel approach to designing and realizing multifunctional materials.

https://doi.org/10.1021/acs.inorgchem.5c03691
Inorg. Chem. 2025, 64, 20796–20803

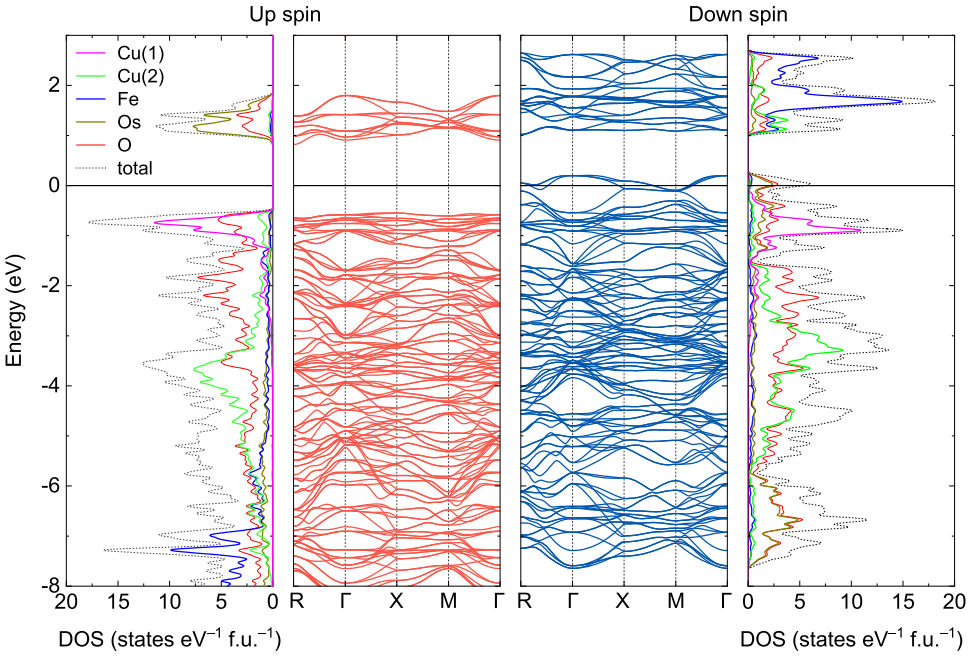

Figure 8. Electronic band structure and partial densities of states (DOS) of CCFOO are determined by DFT + *U* calculations. Fermi energy is at zero.

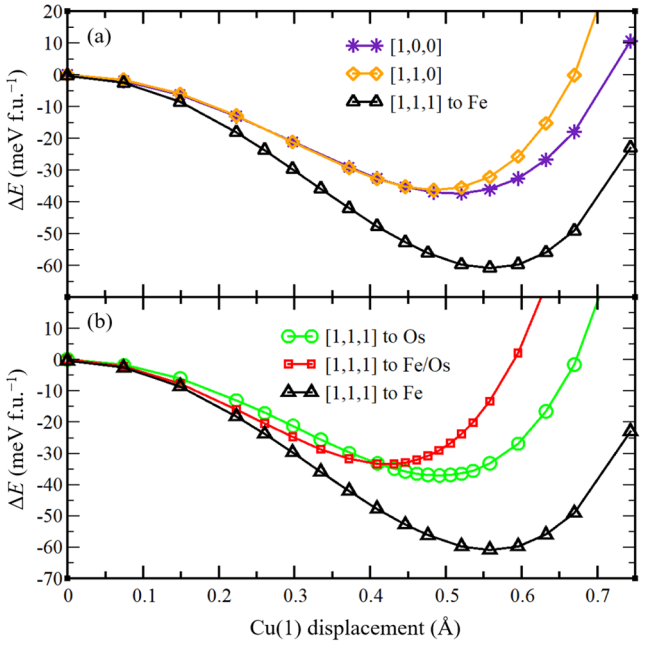

Figure 9. Results of the DFT + *U* calculations. Change in the total energy upon displacement of the Cu(1) ion from the center of the $Cu(1)O_{12}$ icosahedron along various symmetric directions. (a) Along the [100], [110], and one of the [111] directions. (b) Along the [111] direction: both displacements to Os, one to Os and the other to Fe, and both to Fe.

■ ASSOCIATED CONTENT

Accession Codes

Deposition Number 2479123 contains the supplementary crystallographic data for this paper. These data can be obtained free of charge via the joint Cambridge Crystallographic Data Center (CCDC) and Fachinformationszentrum Karlsruhe Access Structures service.

■ AUTHOR INFORMATION

Corresponding Authors

Xiao Wang − *Beijing National Laboratory for Condensed Matter Physics, Institute of Physics, Chinese Academy of Sciences, Beijing 100190, China; Institute of Quantum Materials and Physics, Henan Academy of Sciences, Zhengzhou 450046, China;* orcid.org/0000-0001-8139-4192; Email: xwang@hnas.ac.cn

Sergey V. Streltsov − *M. N. Mikheev Institute of Metal Physics, Ural Branch of Russian Academy of Sciences, 620137 Yekaterinburg, Russia*; Email: streltsov.s@gmail.com

Youwen Long − *Beijing National Laboratory for Condensed Matter Physics, Institute of Physics, Chinese Academy of Sciences, Beijing 100190, China; School of Physical Sciences, University of Chinese Academy of Sciences, Beijing 100049, China; Songshan Lake Materials Laboratory, Dongguan, Guangdong 523808, China;* orcid.org/0000-0002-8587-7818; Email: ywlong@iphy.ac.cn

Authors

Fedor Temnikov − *M. N. Mikheev Institute of Metal Physics, Ural Branch of Russian Academy of Sciences, 620137 Yekaterinburg, Russia*

Xubin Ye − *Beijing National Laboratory for Condensed Matter Physics, Institute of Physics, Chinese Academy of Sciences, Beijing 100190, China;* orcid.org/0000-0002-5739-8318

Maocai Pi − *Beijing National Laboratory for Condensed Matter Physics, Institute of Physics, Chinese Academy of Sciences, Beijing 100190, China; School of Physical Sciences, University of Chinese Academy of Sciences, Beijing 100049, China*

Zhao Pan − *Beijing National Laboratory for Condensed Matter Physics, Institute of Physics, Chinese Academy of Sciences, Beijing 100190, China;* orcid.org/0000-0002-8693-2508

https://doi.org/10.1021/acs.inorgchem.5c03691
Inorg. Chem. 2025, 64, 20796−20803

Weihao Li − *Beijing National Laboratory for Condensed Matter Physics, Institute of Physics, Chinese Academy of Sciences, Beijing 100190, China*
Zhiwei Hu − *Max Planck Institute for Chemical Physics of Solids, 01187 Dresden, Germany;* orcid.org/0000-0003-0324-2227
Chien-Te Chen − *National Synchrotron Radiation Research Center (NSRRC), Hsinchu 300092, Taiwan*
Chang-Yang Kuo − *National Synchrotron Radiation Research Center (NSRRC), Hsinchu 300092, Taiwan; Department of Electrophysics, National Yang Ming Chiao Tung University, Hsinchu 300025, Taiwan;* orcid.org/0000-0003-1968-8020
Cheng Dong − *Beijing National Laboratory for Condensed Matter Physics, Institute of Physics, Chinese Academy of Sciences, Beijing 100190, China*
Yao Shen − *Beijing National Laboratory for Condensed Matter Physics, Institute of Physics, Chinese Academy of Sciences, Beijing 100190, China;* orcid.org/0000-0003-4697-4719
Wenmin Li − *Institute of Quantum Materials and Physics, Henan Academy of Sciences, Zhengzhou 450046, China*

Complete contact information is available at: https://pubs.acs.org/10.1021/acs.inorgchem.5c03691

Notes

The authors declare no competing financial interest.

■ ACKNOWLEDGMENTS

We would like to thank E. Komleva for helping with the calculations of rattling modes. This work was supported by the National Key R&D Program of China (Grant No. 2021YFA1400300), the National Natural Science Foundation of China (Grants No. 12425403, 12261131499, 12304159, 12304268), the High-Level Talent Research Start-Up Project Funding of Henan Academy of Sciences (Project No. 20251827005), the China Postdoctoral Science Foundation (Grant No. 2023M743741), and the open research fund of Beijing National Laboratory for Condensed Matter Physics (2023BNLCMPKF006). The synchrotron X-ray diffraction experiments were performed at SPring-8 with the approval of the Japan Synchrotron Radiation Research Institute (2023B1575). We thank the Russian Science Foundation (Grant 23-42-00069) for supporting the analysis of electronic and magnetic properties, and the studies of structural properties were supported by the Ministry of Science and Higher Education of the Russian Federation through funding the Institute of Metal Physics. The research in Dresden was partially supported by the DFG through SFB 1143. The authors acknowledge the support from the Max Planck-POSTECH-Hsinchu Center for Complex Phase Materials.

■ REFERENCES

(1) Long, Y. W.; Hayashi, N.; Saito, T.; Azuma, M.; Muranaka, S.; Shimakawa, Y. Temperature-induced A−B intersite charge transfer in a A-site-ordered $LaCu_3Fe_4O_{12}$ perovskite. *Nature* **2023**, *458*, 60−63.
(2) Wang, X.; Chai, Y.; Zhou, L.; Cao, H.; Cruz, C.; Yang, J.; Dai, J.; Yin, Y.; Yuan, Z.; Zhang, S.; Yu, R.; Azuma, M.; Shimakawa, Y.; Zhang, H.; Dong, S.; Sun, Y.; Jin, C.; Long, Y. Observation of magnetoelectric multiferroicity in a cubic perovskite system: $LaMn_3Cr_4O_{12}$. *Phys. Rev. Lett.* **2015**, *115*, No. 087601.
(3) Zhang, J.; Ye, X.; Wang, X.; Pan, Z.; Pi, M.; Tang, S.; Dong, C.; Chen, C.-T.; Chen, J.-M.; Kuo, C.-Y.; Hu, Z.; Shen, X.; Yu, X.; Shen, Y.; Yu, R.; Long, Y. Realization of intrinsic colossal magnetoresistance in $Pb(Pb_{1/3}Hg_{2/3})_3Mn_4O_{12}$: an A site-ordered quadruple perovskite oxide. *J. Am. Chem. Soc.* **2025**, *147*, 12644.
(4) Liu, Z.; Zhang, S.; Wang, X.; Ye, X.; Qin, S.; Shen, X.; Lu, D.; Dai, J.; Cao, Y.; Chen, K.; Radu, F.; Wu, W.-B.; Chen, C.-T.; Francoual, S.; Mardegan, J. R. L.; Leupold, O.; Tjeng, L. H.; Hu, Z.; Yang, Y.-f.; Long, Y. Realization of a half metal with a record-high Curie temperature in perovskite oxides. *Adv. Mater.* **2022**, *34*, No. 2200626.
(5) Ye, X.; Yin, Y.; Cao, Y.; Liao, Z.; Wang, X.; Liu, M.; Wang, Q.; Pan, Z.; Hu, Z.; Lin, H.-J.; Chen, C. T.; Pao, C.-W.; Ohresser, P.; Nataf, L.; Baudelet, F.; Yang, W.; Yang, J.; Cheng, J.; Yu, P.; Qiu, X.; Yang, Y.-f.; Xiang, T.; Long, Y. High-temperature ferrimagnetic order triggered metal-to-insulator transition in $CaCu_3Ni_2Os_2O_{12}$. *Nat. Commun.* **2025**, *16*, No. 3746.
(6) Yagi, S.; Yamada, I.; Tsukasaki, H.; Seno, A.; Murakami, M.; Fuji, H.; Chen, H.; Umezawa, N.; Abe, H.; Nishiyama, N.; Mori, S. Covalency-reinforced oxygen evolution reaction catalyst. *Nat. Commun.* **2015**, *6*, No. 8249.
(7) Deng, H.; Liu, M.; Dai, J.; Hu, Z.; Kuo, C.; Yin, Y.; Yang, J.; Wang, X.; Zhao, Q.; Xu, Y.; Fu, Z.; Cai, J.; Guo, H.; Jin, K.; Pi, T.; Soo, Y.; Zhou, G.; Cheng, J.; Chen, K.; Ohresser, P.; Yang, Y.-F.; Jin, C.; Tjeng, L.-H.; Long, Y. Strong enhancement of spin ordering by A-site magnetic ions in the ferrimagnet $CaCu_3Fe_2Os_2O_{12}$. *Phys. Rev. B* **2016**, *94*, No. 024414.
(8) Wang, X.; Liu, M.; Shen, X.; Liu, Z.; Hu, Z.; Chen, K.; Ohresser, P.; Nataf, L.; Baudelet, F.; Lin, H.-J.; Chen, C.-T.; Soo, Y.-L.; Yang, Y.-f.; Jin, C.; Long, Y. High-temperature ferrimagnetic half metallicity with wide spin-up energy gap in $NaCu_3Fe_2Os_2O_{12}$. *Inorg. Chem.* **2019**, *58*, 320.
(9) Wang, X.; Liu, Z.; Ye, X.; Zhou, B.; Hu, Z.; Wang, W.; Yu, R.; Agrestini, S.; Zhou, G.; Chen, K.; Choueikani, F.; Ohresser, P.; Baudelet, F.; Lin, H.-J.; Chen, C.-T.; Tanaka, A.; Weng, S.-C.; Long, Y. Os doping suppressed Cu-Fe charge transfer and induced structural and magnetic phase transitions in $LaCu_3Fe_{4-x}Os_xO_{12}$ (x = 1 and 2). *Inorg. Chem.* **2021**, *60*, 6298.
(10) Wang, X.; Liu, Z.; Deng, H.; Agrestini, S.; Chen, K.; Lee, J.-F.; Lin, H.-J.; Chen, C.-T.; Choueikani, F.; Ohresser, P.; Wilhelm, F.; Rogalev, A.; Tjeng, L. H.; Hu, Z.; Long, Y. Comparative study on the magnetic and transport properties of B-site ordered and disordered $CaCu_3Fe_2Os_2O_{12}$. *Inorg. Chem.* **2022**, *61*, 16929.
(11) Goldschmidt, V. M. Die gesetze der krystallochemie. *Naturwissenschaften* **1926**, *14*, 477.
(12) Chen, W.-t.; Mizumaki, M.; Seki, H.; Senn, M. S.; Saito, T.; Kan, D.; Attifield, J. P.; Shimakawa, Y. A half-metallic A- and B-site-ordered quadruple perovskite oxide $CaCu_3Fe_2Re_2O_{12}$ with large magnetization and a high transition temperature. *Nat. Commun.* **2014**, *5*, No. 3909.
(13) Liu, Z.; Sun, Q.; Ye, X.; Wang, X.; Zhou, L.; Shen, X.; Chen, K.; Nataf, L.; Baudelet, F.; Agrestini, S.; Chen, C.-T.; Lin, H.-J.; Vasili, H. B.; Valvidares, M.; Hu, Z.; Yang, Y.-f.; Long, Y. Quadruple perovskite oxide $LaCu_3Co_2Re_2O_{12}$: a ferrimagnetic half metal with nearly 100% B-site degree of order. *Appl. Phys. Lett.* **2020**, *117*, No. 152402.
(14) Liu, Z.; Wang, X.; Ye, X.; Shen, X.; Bian, Y.; Ding, W.; Agrestini, S.; Liao, S.-C.; Lin, H.-J.; Chen, C.-T.; Weng, S.-C.; Chen, K.; Ohresser, P.; Nataf, L.; Baudelet, F.; Sheng, Z.; Francoual, S.; Mardegan, J. R. L.; Leupold, O.; Li, Z.; Xi, X.; Wang, W.; Tjeng, L. H.; Hu, Z.; Long, Y. Observation of A-site antiferromagnetic and B-site ferrimagnetic orderings in the quadruple perovskite oxide $CaCu_3Co_2Re_2O_{12}$. *Phys. Rev. B* **2021**, *103*, No. 014414.
(15) Zhang, J.; Liu, Z.; Ye, X.; Wang, X.; Lu, D.; Zhao, H.; Pi, M.; Chen, C.-T.; Chen, J.-L.; Kuo, C.-Y.; Hu, Z.; Yu, X.; Zhang, X.; Pan, Z.; Long, Y. High-pressure synthesis of quadruple perovskite oxide CaCu3$Cr_2Re_2O_{12}$ with a high ferrimagnetic Curie temperature. *Inorg. Chem.* **2024**, *63*, 3499.
(16) Syono, Y.; Akimoto, S.-I.; Endoh, Y. High pressure synthesis of ilmenite and perovskite type $MnVO_3$ and their magnetic properties. *J. Phys. Chem. Solids* **1971**, *32*, 243.

(17) Markkula, M.; Arevalo-Lopez, A. M.; Kusmartseva, A.; Rodgers, J. A.; Ritter, C.; Wu, H.; Attfield, J. P. Incommensurate spin order in the metallic perovskite $MnVO_3$. *Phys. Rev. B* **2011**, *84*, No. 094450.
(18) Li, M.-R.; Retuerto, M.; Deng, Z.; Stephens, P. W.; Croft, M.; Huang, Q.; Wu, H.; Deng, X.; Kotliar, G.; Sánchez-Benítez, J.; Hadermann, J.; Walker, D.; Greenblatt, M. Giant magnetoresistance in the half-metallic double-perovskite ferrimagnet Mn_2FeReO_6. *Angew. Chem., Int. Ed.* **2015**, *54*, 12069.
(19) Arévalo-López, A. M.; McNally, G. M.; Attfield, J. P. Large magnetization and frustration switching of magnetoresistance in the double-perovskite ferrimagnet Mn_2FeReO_6. *Angew. Chem., Int. Ed.* **2015**, *54*, 12074.
(20) Li, M.-R.; Hodges, J. P.; Retuerto, M.; Deng, Z.; Stephens, P. W.; Croft, M. C.; Deng, X.; Kotliar, G.; Sánchez-Benítez, J.; Walker, D.; Greenblatt, M. Mn_2MnReO_6: synthesis and magnetic structure determination of a new transition-metal-only double perovskite canted antiferromagnet. *Chem. Mater.* **2016**, *28*, 3148.
(21) Li, M.-R.; McCabe, E. E.; Stephens, P. W.; Croft, M.; Collins, L.; Kalinin, S. V.; Deng, Z.; Retuerto, M.; Gupta, A. S.; Padmanabhan, H.; Gopalan, V.; Grams, C. P.; Hemberger, J.; Orlandi, F.; Manuel, P.; Li, W.-M.; Jin, C.-Q.; Walker, D.; Greenblatt, M. Magnetostriction-polarization coupling in multiferroic Mn_2MnWO_6. *Nat. Commun.* **2017**, *8*, No. 2037.
(22) Frank, C. E.; McCabe, E. E.; Orlandi, F.; Manuel, P.; Tan, X.; Deng, Z.; Croft, M.; Cascos, V.; Emge, T.; Feng, H. L.; Lapidus, S.; Jin, C.; Wu, M.; Li, M. R.; Ehrlich, S.; Khalid, S.; Quackenbush, N.; Yu, S.; Walker, D.; Greenblatt, M. Mn_2CoReO_6: a robust multi-sublattice antiferromangnetic with small A-site cations. *Chem. Commun.* **2019**, *55*, 3331.
(23) Wang, X.; Zhang, J.; Pan, Z.; Lu, D.; Pi, M.; Ye, X.; Dong, C.; Chen, J.; Chen, K.; Radu, F.; Francoual, S.; Agrestini, S.; Hu, Z.; Chang, C.-F.; Tanaka, A.; Yamaura, K.; Shen, Y.; Long, Y. X-ray absorption spectroscopic study of the transition-metal-only double perovskite oxide Mn_2CoReO_6. *J. Phys. Chem. C* **2024**, *128*, 15668.
(24) Akizuki, Y.; Yamada, I.; Fujita, K.; Nishiyama, N.; Irifune, T.; Yajima, T.; Kageyama, H.; Tanaka, K. A-site-ordered perovskite $MnCu_3V_4O_{12}$ with a 12-coordinated manganese(II). *Inorg. Chem.* **2013**, *52*, 11538.
(25) Akizuki, Y.; Yamada, I.; Fujita, K.; Taga, K.; Kawakami, T.; Mizumaki, M.; Tanaka, K. Rattling in the quadruple perovskite $CuCu_3V_4O_{12}$. *Angew. Chem., Int. Ed.* **2015**, *54*, 10870.
(26) Guo, J.; Wang, S.; Li, W.; Lu, D.; Ye, X.; Liu, Z.; Qin, S.; Wang, X.; Hu, Z.; Lin, H.-J.; Chen, C.-T.; Wan, J.; Zhang, Q.; Long, Y. A-site Mn^{2+} tuned magnetism and electrical transport properties in the transition-metal-only perovskite oxide $MnCu_3Mn_4O_{12}$. *Phys. Rev. B* **2022**, *105*, No. 054409.
(27) Keppens, V.; Mandrus, D.; Sales, B. C.; Chakoumakos, B. C.; Dai, P.; Coldrea, R.; Maple, M. B.; Gajewski, D. A.; Freeman, E. J.; Bennington, S. Localized vibrational modes in metallic solids. *Nature* **1998**, *395*, 876.
(28) Beekman, M.; Morelli, D. T.; Nolas, G. S. Better thermoelectrics through glass-like crystals. *Nat. Mater.* **2015**, *14*, 1182.
(29) Rietveld, H. M. A profile refinement method for nuclear and magnetic structures. *J. Appl. Crystallogr.* **1969**, *2*, 65.
(30) Von Dreele, R. B. Quantitative texture analysis by Rietveld refinement. *J. Appl. Crystallogr.* **1997**, *30*, 517.
(31) Kresse, G.; Joubert, D. From ultrasoft pseudopotentials to the projector augmented-wave method. *Phys. Rev. B* **1999**, *59*, 1758.
(32) Perdew, J. P.; Burke, K.; Ernzerhof, M. Generalized gradient approximation made simple. *Phys. Rev. Lett.* **1996**, *77*, 3865.
(33) Anisimov, V. I.; Zaanen, J.; Andersen, O. K. Band theory and Mott insulators: Hubbard *U* instead of Stoner *I*. *Phys. Rev. B* **1991**, *44*, 943.
(34) Franchini, C.; Kovacik, R.; Marsman, M.; Murthy, S. S.; He, J.; Ederer, C.; Kresse, G. Maximally localized Wannier functions in $LaMnO_3$ within PBE + *U*, hybrid functionals and partially self-consistent GW: an efficient route to construct *ab initio* tight-binding parameters for e_g perovskites. *J. Phys.:Condens. Matter* **2012**, *24*, No. 235602.
(35) Monkhorst, H. J.; Pack, J. D. Special points for Brillouin-zone integrations. *Phys. Rev. B* **1976**, *13*, 5188.
(36) Brown, I. D.; Altermatt, D. Bond-valence parameters obtained from a systematic analysis of the inorganic crystal structure database. *Acta. Cryst. B* **1985**, *41*, 244.
(37) Chen, J.; Wang, X.; Hu, Z.; Tjeng, L. H.; Agrestini, S.; Valvidares, M.; Chen, K.; Nataf, L.; Baudelet, F.; Nagao, M.; Inaguma, Y.; Belik, A. A.; Tsujimoto, Y.; Matsushita, Y.; Kolodiazhnyi, T.; Sereika, R.; Tanaka, M.; Yamaura, K. Enhanced magnetization of the highest-T_C ferrimagnetic oxide Sr_2CrOsO_6. *Phys. Rev. B* **2020**, *102*, No. 184418.
(38) Tjeng, L. H.; Chen, C. T.; Cheong, S.-W. Comparative soft-x-ray resonant-photoemission study on $Bi_2Sr_2CaCu_2O_8$, CuO, and Cu_2O. *Phys. Rev. B* **1992**, *45* (R), 8205.
(39) Hu, Z.; Drechsler, S.-L.; Malek, J.; Rosner, H.; Neudert, R.; Knupfer, M.; Golden, M. S.; Fink, J.; Karpinski, J.; Kaindl, G.; Hellwig, C.; Jung, Ch. *Europhys. Lett.* **2002**, *59*, 135.
(40) Grioni, M.; Goedkoop, J. B.; Schoorl, R.; de Groot, F. M. F.; Fuggle, J. C.; et al. Studies of copper valence states with Cu L_3 x-ray-absorption spectroscopy. *Phys. Rev. B* **1989**, *39*, 1541.
(41) Feng, H. L.; Calder, S.; Ghimire, M. P.; Yuan, Y.-H.; Shirako, Y.; Tsujimoto, Y.; Matsushita, Y.; Hu, Z. W.; Kuo, C.-Y.; Tjeng, L. H.; Pi, T.-W.; Soo, Y.-L.; He, J.; Tanaka, M.; Katsuya, Y.; Richter, M.; Yamaura, K. Ba_2NiOsO_6: a Dirac-Mott insulator with ferromagnetism near 100 K. *Phys. Rev. B* **2016**, *94*, No. 235158.
(42) Kobayashi, K.-I.; Kimura, T.; Sawada, H.; Terakura, K.; Tokura, Y. Room-temperature magnetoresistance in an oxide material with an ordered double-perovskite structure. *Nature* **1998**, *395*, 677.
(43) Takahata, K.; Iguchi, Y.; Tanaka, D.; Itoh, T.; Terasaki, I. Low thermal conductivity of the layered oxide $(Na,Ca)Co_2O_4$: another example of a phonon glass and an electron crystal. *Phys. Rev. B* **2000**, *61*, 12551.
(44) Satake, A.; Tanaka, H.; Ohkawa, T.; Fujii, T.; Terasaki, I. Thermal conductivity of the thermoelectric layered cobalt oxides measured by the Harman method. *J. Appl. Phys.* **2004**, *96*, 931.
(45) Mandrus, D.; Thompson, J. R.; Gaal, R.; Forro, L.; Bryan, J. C.; Chakoumakos, B. C.; Woods, L. M.; Sales, B. C.; Fishman, R. S.; Keppens, V. Continuous metal-insulator transition in the pyrochlore $Cd_2Os_2O_7$. *Phys. Rev. B* **2001**, *63*, No. 195104.
(46) Takahata, K.; Ichiro, T. Thermal conductivity of A_xBO_2-type layered oxides $Na_{0.77}MnO_2$ and $LiCoO_2$. *Jpn. J. Appl. Phys.* **2002**, *41*, 763.
(47) Coey, J. M. D.; Sanvito, S. Magnetic semiconductors and half-metals. *J. Phys. D:Appl. Phys.* **2004**, *37*, 988.
(48) Pchelkina, Z. V.; Komleva, E. V.; Irkhin, V. Yu.; Long, Y.; Streltsov, S. V. Rattling phonon modes in quadruple perovskites. *JETP Lett.* **2023**, *118*, 738.
(49) Iwamoto, K.; Mori, T.; Kajitani, S.; Matsumoto, H.; Toyota, N.; Suekuni, K.; Avila, M. A.; Saiga, Y.; Takabatake, T. Optical conductivity spectra of rattling phonons and charge carriers in the type-VIII clathrate $Ba_8Ga_{16}Sn_{30}$. *Phys. Rev. B* **2013**, *88*, No. 104308.
(50) Wang, S.; Salvador, J. R.; Yang, J.; Wei, P.; Duan, B.; Yang, J. High-performance *n*-type $Yb_xCo_4Sb_{12}$: from partially filled skutterudites towards composite thermoelectrics. *NPG Asia Mater.* **2016**, *8*, No. e285.

https://doi.org/10.1021/acs.inorgchem.5c03691
Inorg. Chem. 2025, 64, 20796−20803